# Geochemistry, Geophysics, Geosystems®

**AGU** ADVANCING EARTH AND SPACE SCIENCE

**Key Points:**
- A new Moho map was constructed from available seismic data to improve thermo-compositional modeling of the African cratonic lithosphere
- Lithosphere of the West African, central to northern Congo, and Zimbabwe cratons is cold, up to 250 km thick, and chemically depleted
- Hot, thin (<200 km) and mostly undepleted lithosphere of Uganda, Tanzania, southern Congo, and Kaapvaal cratons indicates refertilization

**Correspondence to:**
N.-P. Finger,
finger@gfz-potsdam.de

**Author Contributions:**
**Conceptualization:** N.-P. Finger, M. K. Kaban
**Data curation:** N.-P. Finger, W. D. Mooney
**Formal analysis:** N.-P. Finger
**Funding acquisition:** M. K. Kaban, M. Thomas
**Investigation:** N.-P. Finger
**Methodology:** N.-P. Finger, M. K. Kaban, M. Tesauro
**Project Administration:** M. K. Kaban, M. Thomas
**Resources:** M. Thomas
**Software:** N.-P. Finger, M. K. Kaban
**Supervision:** M. K. Kaban

# A Thermo-Compositional Model of the African Cratonic Lithosphere

**N.-P. Finger[1,2]** [ID], **M. K. Kaban[1]** [ID], **M. Tesauro[3,4]** [ID], **W. D. Mooney[5]** [ID], and **M. Thomas[1,2]**

[1]German Research Centre for Geosciences, Potsdam, Germany, [2]FU Berlin, Berlin, Germany, [3]University of Trieste, Trieste, Italy, [4]University of Utrecht, Utrecht, The Netherlands, [5]US Geological Survey, Menlo Park, CA, USA

**Abstract** Recently, the continually increasing availability of seismic data has allowed high-resolution imaging of lithospheric structure beneath the African cratons. In this study, S-wave seismic tomography is combined with high resolution satellite gravity data in an integrated approach to investigate the structure of the cratonic lithosphere of Africa. A new model for the Moho depth and data on the crustal density structure is employed along with global dynamic models to calculate residual topography and mantle gravity residuals. Corrections for thermal effects of an initially juvenile mantle are estimated based on S-wave tomography and mineral physics. Joint inversion of the residuals yields necessary compositional adjustments that allow to recalculate the thermal effects. After several iterations, we obtain a consistent model of upper mantle temperature, thermal and compositional density variations, and Mg# as a measure of depletion, as well as an improved crustal density model. Our results show that thick and cold depleted lithosphere underlies West African, northern to central eastern Congo, and Zimbabwe Cratons. However, for most of these regions, the areal extent of their depleted lithosphere differs from the respective exposed Archean shields. Meanwhile, the lithosphere of Uganda, Tanzania, most of eastern and southern Congo, and the Kaapvaal Craton is thinner, warmer, and shows little or no depletion. Furthermore, the results allow to infer that the lithosphere of the exposed Archean shields of Congo and West African cratons was depleted before the single blocks were merged into their respective cratons.

**Plain Language Summary** Cratons are the ancient cores of continents that, with few exceptions, are underlain by a cold, strong lithospheric root with a thickness of about 250 km. The physical properties of lithospheric roots, principally temperature and composition, shed light on the origin and evolution of the most ancient portions of the Earth's lithosphere, the Precambrian cratons. We use an iterative method to process S-wave seismic tomography and satellite gravity data to calculate the thermal and compositional state of the lithosphere. Our results reveal great diversity in the thickness and physical properties of the African lithosphere. The West African, northern Congo, and Zimbabwe cratons are underlain by relatively cold, thick and chemically depleted lithosphere. In contrast, the Uganda, Tanzania, southern Congo, and Kaapvaal cratons are warmer, thinner and have a less depleted (or non-depleted) composition, indicating either refertilization (metasomatism) or formation in a non-depleted state. These results document the formation of the Africa continent during the past 3.7 Ga from a diverse collection of cratons, each with a unique evolutionary history.

## 1. Introduction

Cratons are the ancient continental cores, around which continents accrete and grow. They are stable for billions of years, and due to their geologic evolution often provide an abundancy of resources, for example, rare earth elements and diamonds. Cratons are usually underlain by thick continental lithosphere, their so-called "roots", which can reach up to about 250 km into the Earth (e.g., Steinberger & Becker, 2018). With a few exceptions (Kaban et al., 2015), these roots resist mantle convection, and thus deviate mantle flow. Therefore, a better understanding of cratons, their evolution and dynamics may provide further insight to large-scale dynamic and tectonic processes. Cratons appear to be buoyant with respect to the underlying mantle despite the fact that their long-term cooling causes an increase in density. A commonly cited explanation is the iso-pycnic hypothesis (Jordan, 1978) that is based on the counter-balancing effect of chemical buoyancy. The density increase caused by reduced temperatures is balanced by density decrease from depletion in heavy constituents, mostly iron (Fe; Griffin, O'Reilly, Natapov, & Ryan, 2003). Depletion is commonly measured by means of Mg#, the percentage of Magnesium (Mg) in the total amount of Mg and Fe ($100*Mg/(Mg + Fe)$) in mantle minerals. Mg#s around 89 are common for fertile mantle rocks, while strongly depleted samples exhibit values around 94 (Griffin, O'Reilly,

**Validation:** N.-P. Finger, M. K. Kaban,
M. Tesauro, W. D. Mooney
**Visualization:** N.-P. Finger
**Writing – original draft:** N.-P. Finger,
M. K. Kaban, W. D. Mooney
**Writing – review & editing:** N.-P.
Finger, M. K. Kaban, M. Tesauro, W. D.
Mooney, M. Thomas

Abe, et al., 2003; McDonough & Sun, 1995). Still, despite being a long-time focus of geoscientific studies, in a global perspective, various cratons have been studied to very different extents and several aspects concerning their physical properties are still under debate (e.g., Celli et al., 2020; Mooney & Vidale, 2003). On the African continent, a large body of geologic, geochemical, and geophysical data and numerous publications exist for the Kaapvaal and adjacent Zimbabwe cratons, along with a large array of seismic stations (Globig et al., 2016). Yet, lithospheric thickness of these cratons is still a matter of debate (White-Gaynor et al., 2021). Meanwhile, much fewer seismic stations and other data are available for the significantly larger Congo and West African cratons.

However, employing seismic tomography and satellite gravity data allows an assessment of the thermal and compositional state of the cratonic lithosphere, even for very remote or not accessible areas like Antarctica (e.g., Haeger et al., 2019). On the one hand, seismic velocities provide a solid and widely used basis for temperature estimates of the lithosphere (Cammarano et al., 2003; Steinberger & Becker, 2018) since they are primarily governed by thermal variations (Goes et al., 2000). In comparison, compositional variations have a rather minor influence on seismic velocities (e.g., Schutt & Lesher, 2010). Both thermal and compositional variations cause density variations, which can be detected, but not separated by gravity measurements. Thus, integrated modeling of gravity and seismic data profits from their respective advantages while reducing the disadvantages. A respective approach (Kaban et al., 2014; Tesauro et al., 2014a) was recently used to assess the thermal and compositional state of cratonic lithosphere of several continents, for example, South America (Finger, Kaban, Tesauro, Haeger, et al., 2021), Antarctica (Haeger et al., 2019), and Australia (Tesauro et al., 2020). The method yields self-consistent thermal and compositional results for the mantle lithosphere from the Moho down to about 325 km. Despite providing sophisticated indications for the current state and depth extent of cratonic lithosphere, the results can also be a basis for further studies. For example, results for Antarctica (Haeger et al., 2019) were used to calculate decompositional gravity anomalies in an attempt to determine the thickness of sediments beneath the ice (Haeger & Kaban, 2019).

As mentioned above, the African continent comprises several cratons (Figure 1) whose lithospheric thickness, physical state, and evolution are still a matter of debate (Boyce et al., 2021; Celli et al., 2020; Hu et al., 2018; Jessell et al., 2016; White-Gaynor et al., 2021). Here, we apply the previously mentioned approach to model the thermal and compositional state of the cratonic lithosphere of Africa. First, we produce a new, purely seismic model of depth to the Moho from available data (Globig et al., 2016; Mooney, 2015 with updates up to 2019), which is then used in calculation of residual topography and correction of the initial gravity field (EIGEN-6C4, Förste et al., 2014) for crustal effects. Second, assuming an initially juvenile mantle, we determine thermal density variations and temperatures from S-wave tomography (Celli et al., 2020) by means of mineral physics parameters and equations (Cammarano et al., 2003; Stixrude & Lithgow-Bertelloni, 2005). After correcting the gravity and residual topography for these thermal effects, the two fields are jointly inverted for further density variations. Interpreting these to be of compositional origin, the assumed bulk composition and proportions of mineral phases are updated toward those of a depleted mantle. This allows to refine the estimation of thermal variations and temperatures, and iteratively improve the model. The final model provides self-consistent fields of temperature, thermal and compositional density variations, and Mg# as a measure of depletion. Moreover, the results allow to determine an improved model of average crustal densities, and to assess to which extent interpolation of depth to Moho affects the results of the integrated mantle model.

## 1.1. Geology Overview

Begg et al. (2009) and references therein provide a detailed summary of the main terranes, belts, and basins of the African continent. Here, a simplified overview based on their work is provided except where noted. The cratonic part of Africa, on which this study focuses, consists of the West African craton, the cratons from the central African Oubanguides belt southwards, and most of their surrounding Proterozoic fold belts (white polygon in Figure 1). The non-cratonic part is constituted by wide parts of the extensive "Saharan" domain, namely the West African mobile zone and the East Saharan metacraton, as well as the East African orogenic zone down to the eastern border of the Tanzania craton. While cratons are inferred to occupy a significant portion of the cratonic region, only some of their areas are actually exposed Archean shields, while most of their surface is covered by sedimentary basins. In the case of the West African craton, the northern Reguibat and southern Man-Leo shields are separated by the Proterozoic Taoudeni basin covering the craton's central area. Recent S-wave tomography (Celli et al., 2020) indicates two separate roots. The Congo Craton in central Afrika hosts
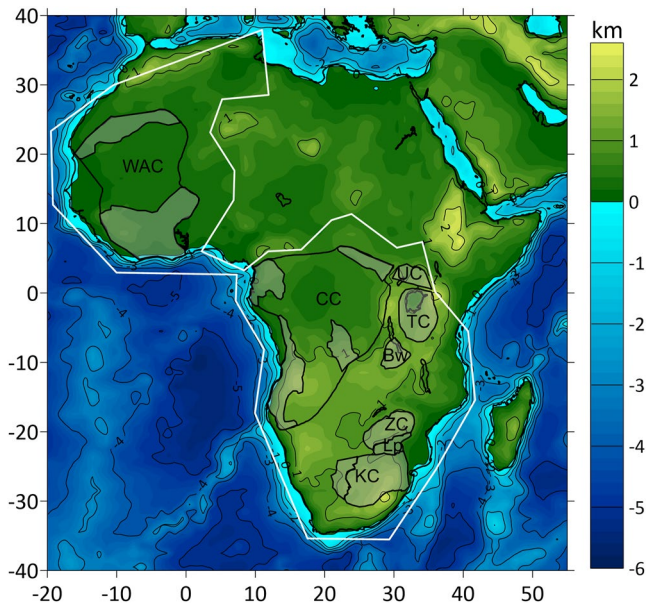
**Figure 1.** Topography and bathymetry of Africa and surrounding area. Numbers indicate elevation contours in km. This study is focused on the cratonic regions denoted by the white polygon. Mostly exposed cratons are indicated by black outlines, with Archean shields and microcontinents shaded gray (Begg et al., 2009). WAC, West African craton; CC, Congo craton; UC, Uganda craton; TC, Tanzania craton; Bw, Bangweulu block; ZC, Zimbabwe craton; Lp, Limpopo belt; and KC, Kaapvaal craton.

four Archean shield areas, parts of which are probably covered by the Congo basin: the Gabun-Cameroon in the Northwest, Bomu-Kibali in the Northeast, Kasai in the central East, and Angolan along the western border south of the Gabun-Cameroon. Begg et al. (2009) infer different ages and a unique evolution of the four shields. However, Congo craton lithosphere appeared as a single large block in tomographies (e.g., Fishwick, 2010; Schaeffer & Lebedev, 2013) until recent advances allowed to image separate root structures (Celli et al., 2020). To the East, an emerging plate boundary now separates the Congo craton from the 2.9 to 2.8 Ga old Uganda and Tanzania cratons, which have been accreted to it during 1.8 Ga paleo-Kibaran orogeny, together with the Bangweulu block, a Neoarchean microcontinent. Tomography (Celli et al., 2020) indicates that the Uganda and Tanzania cratons both lack a deep root. For the Tanzania craton, an east-to-west increase of lithosphere thickness (Boyce et al., 2021) and presence of about 30 Ma old kimberlites (Tappe et al., 2018) point to a geologically recent root loss due to plume impingement that also initiated the East African rift system (EARS). The Kaapvaal and Zimbabwe cratons collided 2.6–2.7 Ga, capturing the Limpopo microcontinent between them and currently form the South African craton. Several large igneous provinces (LIPs) were emplaced on top or in the vicinity of the cratons: the Bushveld (around 2.05 Ga) and Karoo (180 Ma, Giuliani et al., 2014) on the Kaapvaal craton, Etendeka (135 Ma, Morgan, 1983) on the Angolan shield of the Congo craton, along with the formation of the EARS next to the Tanzania craton (30 Ma until today, Ebinger & Sleep, 1998), and the Central Atlantic magmatic province (CAMP, 200 Ma, Wilson, 1997) close to the West African craton. CAMP, Etendeka, and Karoo preceded or accompanied the separation from South America and Antarctica, ending the Pangean supercontinent. Emplacement of such LIPs is generally thought to be caused by mantle plumes (e.g., Ebinger & Sleep, 1998), which are among the few geologic processes able to significantly affect or even erode cratonic lithosphere (Lee et al., 2011).

## 2. Methods

### 2.1. Depth to the Moho and Crustal Model

The method employed in this work (Figure 2), which is the same as in our recent study of the South American cratonic regions (Finger, Kaban, Tesauro, Haeger, et al., 2021), starts with interpolation of depth to the Moho. An accurate as possible estimate is critical to later obtain the best-fitting upper mantle model. Various Moho depth models have been presented for Africa over the past decades, either in a regional (e.g., Globig et al., 2016; Haas et al., 2021; Pasyanos & Nyblade, 2006; Tugume et al., 2013) or global context (e.g., Laske et al., 2013; Pasyanos et al., 2014) and based on different data and modeling techniques. However, a purely seismic determination is desired for the approach applied here, but previous seismic models show large differences (van der Meijde et al., 2015). Therefore, we calculate a new model of depth to the Moho via the method of Stolk et al. (2013) using topography (Amante & Eakins, 2009), sediment (Laske et al., 2013), and seismic data. For the latter, we augmented the compilation published by Globig et al. (2016) with data from the Global Seismic Catalog (GSC; Mooney, 2015 with updates up to 2019). The subset of GSC data used here is included in the data publication associated with this study (Finger, Kaban, Tesauro, Mooney, & Thomas, 2021). The method is based on the reasonable assumption that measurements of crustal thickness (including topography) or depth to the Moho (at sea-level) reflect isostatic topographic effects. Subtracting these from data reduces their variance and thus variance of the subsequent interpolation. Afterward, effects can be restored to the interpolated field. This way, interpolated depth to the Moho follows main topographic features in areas of sparse data. Seismic measurements are binned to $1° \times 1°$ cells to reduce the effects of outliers. Then, determination of isostatic effects starts with calculating adjusted topography, which would be the residing topography if sediments and water were compacted to the density of topography (2.67 g/cm³). Due to a lack of relevant data, it was not possible to create a sediment density model like for South America (Finger et al., 2020, 2021). Instead, data for the sedimentary layers from
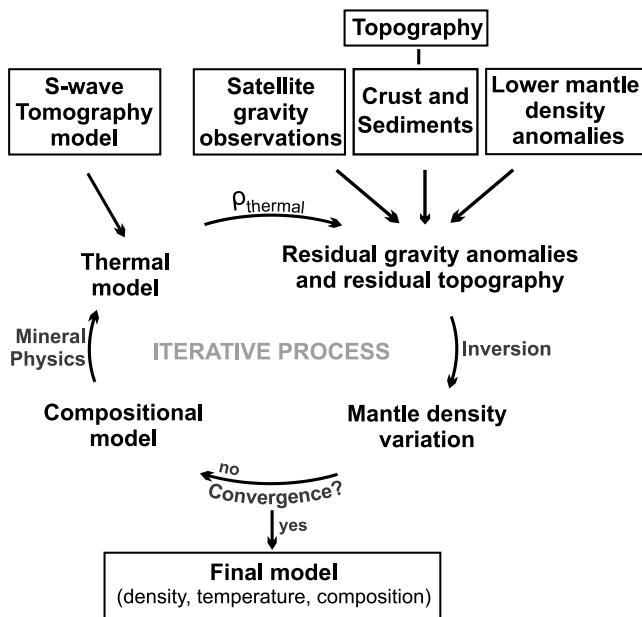
**Figure 2.** Sketch of the iterative approach that integrates multiple constraints (modified from Haeger et al., 2019). To enable the iterative process, S-wave velocities are converted into a thermal model. In addition, calculation of depth to the Moho (Section 2.2) permits the determination of crustal effects, and thus residual mantle gravity and residual topography. After correction for effects of the thermal model, these are jointly inverted to identify further necessary density variations that are interpreted to be of compositional origin. Then, the initial thermal model is updated and the next iteration starts. Convergence is reached when the inversion does not indicate changes of Mg# > 0.1.

CRUST1.0 (Laske et al., 2013) are used. The type of isostacy is not relevant, since the effects will be restored to the interpolated field (Kaban, Stolk, et al., 2016; Stolk et al., 2013). Here, local Airy Isostasy is assumed. After removing the isostatic effects from the binned data, outliers are removed by hold-one-out cross-correlation. Depth to the Moho is interpolated by means of ordinary kriging as implemented in PyKrige (Murphy et al., 2020), treating the binned measurements as exact. Finally, the isostatic correction is restored to the interpolated field. Later, interpolation results in areas of scarce or no data can be assessed using the results of the iterative scheme (Kaban, El Khrepy, & Al-Arifi, 2016). Since the iterative approach requires global fields, results for depth to Moho were merged into a global map consisting of CRUST1.0 (Laske et al., 2013) with updates from previous studies for most continents (Finger, Kaban, Tesauro, Haeger, et al., 2021; Kaban, Stolk, et al., 2016; Tesauro et al., 2014b).

As was demonstrated in previous studies (e.g., Finger, Kaban, Tesauro, Haeger, et al., 2021), the gravity effect of the crystalline crust is very significant. In many regions, it can be estimated using measured crustal thickness and converting seismic velocities to densities (e.g., Kaban, El Khrepy, Al-Arifi, et al., 2016). Unfortunately, for Africa this is hardly possible because reliable determinations of crustal velocities are even more sparse than the Moho determinations. For example, the receiver functions usually provide reliable depth to Moho determinations but not crustal seismic velocities. This problem regarding sparse data was previously addressed in the study of South America (Finger, Kaban, Tesauro, Haeger, et al., 2021). Therefore, here we use a similar approach to estimate the correction for the crystalline crust. The initial model is chiefly based on the tectonic type and age of specific structures taking into account their lithology as in the CRUST1.0 model (Laske et al., 2013), including sediments. Here, we employ the model LITHO1.0 (Pasyanos et al., 2014) for the initial density of the crystalline crust. In LITHO1.0, the crustal parameters from CRUST1.0 have been substantially corrected using a joint inversion with surface waves tomography data to fit high-resolution surface wave dispersion maps. However, at a later stage, we further improve their model of crystalline crust densities with results from the joint inversion.

## 2.2. Correction for Crustal and Deep Mantle Effects

After construction of the crustal model, we compute its effects and remove these from the observed topography and gravity field. The free air gravity disturbances, which are used as the initial field, are taken from EIGEN-6C4 (Förste et al., 2014). Although the model is based on a combination of satellite and ground/airborne determinations, for the resolution of this study (1° × 1°) it is determined only from satellite data. Using these data, the initial field has sufficient resolution for the whole study area.

We compute the effect of density deviations from a 1D reference model (Table 1) as in previous studies (e.g., Finger, Kaban, Tesauro, Haeger, et al., 2021; Kaban, Stolk, et al., 2016; Mooney & Kaban, 2010). Although the choice of such a model only causes a constant shift of the computed fields, which is not considered here (Mooney & Kaban, 2010), using the same reference model provides a useful opportunity for comparison with results obtained in previous studies for different continents. The initial density of topography is 2.67 g/cm³. Later on, effects of low-density sediments have also been considered. The ocean water density is 1.03 g/cm³.

The gravity effects of all crustal layers were estimated by a 3D approach on the sphere as described in previous studies (Kaban et al., 2015; Kaban, Stolk, et al., 2016). Comparison with other independent methods has shown that its accuracy is within few mGal (Root et al., 2016), which is sufficient for the present study. Even remote structures, especially at large depths, can produce a significant gravity effect in the study area. Therefore, the calculations

**Table 1**
*1D Reference Model of the Crust and Uppermost Mantle*

|  | Upper crustal layer | Lower crustal layer | Subcrustal layer |
|---|---|---|---|
| Depth (km) | 0–15 | 15–40 | 40–75 |
| Density (g/cm³) | 2.7 | 2.94 | 3.32 |

were made for a global model (e.g., Mooney & Kaban, 2010). Outside the study area, we employed CRUST1.0 (Laske et al., 2013), which was improved by several continental models with higher resolution (e.g., Finger, Kaban, Tesauro, Haeger, et al., 2021; Kaban, Stolk, et al., 2016; Mooney & Kaban, 2010). Since far-field effects depend only on large-scale structures, possible uncertainties of the global model do not affect the obtained results remarkably.

In addition to the residual mantle gravity field, the residual topography has also been estimated based on the same data on crustal structure. The residual topography is the part of topography that is not fully compensated by the crustal heterogeneity. For the crust, the residual topography has been computed by assuming local isostatic conditions (Kaban, Stolk, et al., 2016). For the mantle, the effect on topography has been computed in a dynamic environment by considering mantle viscosity as described in Kaban, El Khrepy et al. (2016). Effects of deeper mantle density anomalies (below 325 km) are removed from the two fields by means of global dynamic models based on tomography (S40RTS, Ritsema et al., 2011), as was done in previous studies (Kaban et al., 2015; Kaban, El Khrepy, Al-Arifi et al., 2016). Although existing tomography models show some differences, all global dynamic models can be fit to the observed geoid heights via appropriate velocity-to-density scaling factors and assumed viscosity of the mantle. Therefore, the gravity effect of the mantle and dynamic topography should be similar for all models. The most significant effect of the deep layers is found in the Red Sea and Afar triple junction. Here, it corresponds well to the detailed model of the Middle East and surrounding areas (Kaban, El Khrepy, Al-Arifi et al., 2016). In other areas of Africa, these effects are only present in the very long wavelengths and in the cratonic area they represent only quasilinear trends (Kaban, El Khrepy, Al-Arifi et al., 2016). Therefore, they do not notably affect the results presented here.

## 2.3. Initial Mantle Model

After determination of the residual mantle fields, the initial mantle model is constructed. It consists of six layers that are centered at 50–300 km depth with an interval of 50 km and 1° lateral resolution. Initially, a juvenile fertile mantle with Mg# 89 is assumed, representing a bulk composition of 58.5% Olivine (Ol), 11.5% Clinopyroxene (CPX), 15% Orthopyroxene (OPX), and 15% Garnet (Gt; Griffin, O'Reilly, Abe, et al., 2003). Thus, Mg# describes both the composition and the proportions of each mineral's Mg and Fe endmembers. Based on this composition, density $\rho$ and shear modulus $\mu$ of the mineral assemblage are forward calculated for a range of pressures corresponding to depths between 50 and 300 km (according to PREM, Dziewonski & Anderson, 1981), and for temperatures up to 1800°C. This is done for each mineral by using the mineral physics approach of Stixrude and Lithgow-Bertelloni (2005). Respective mineral parameters are taken from Stixrude and Lithgow-Bertelloni (2005) and Cammarano et al. (2003). Bulk density is obtained as the volumetric sum, while bulk shear modulus is calculated by Voigt-Reuss-Hill averaging. Then, synthetic S-wave velocities are determined via $V_{s,syn} = \sqrt{\frac{\mu}{\rho}}$. Anelastic effects are considered by using models of Cammarano et al. (2003), based on the homologous temperature approach. Their model *Q3* is applied to the part of the study area that is expected to be mostly cratonic (white polygon in Figure 1), while their model *Q4* is used for the other areas. *Q3* weakly reduces the linearity of the relationship between seismic velocity and temperature. Thus, it is more representative of the dry, highly viscous upper mantle expected to underlie the cratons. In contrast, *Q4* enhances the effect of anelasticity by assuming a rather hydrous, metasomatized mantle, which likely characterizes the other areas. Finally, temperatures and corresponding thermal density variations in the upper mantle are determined as those values, whose synthetic S-wave velocities best fit the recent seismic tomography AF2019 (Celli et al., 2020).

## 2.4. Iterative Process and Final Mantle Model

The iterative process begins with removing the effects of the previously calculated thermal variations from the residual mantle gravity and residual topography. Then, the thermally corrected fields are jointly inverted to identify further density variations. Since gravity and residual topography react differently to mass changes (Kaban & Mooney, 2001), use of both fields principally improves vertical resolution of the inversion (Kaban, El Khrepy, & Al-Arifi, 2016). The inversion is performed in spherical harmonics and includes a regularization term to ensure that density changes are kept minimal. A seventh layer centered at 15 km is added to cover for density variations not included in the initial crustal model. Mantle density variations proposed by the joint inversion are assumed to
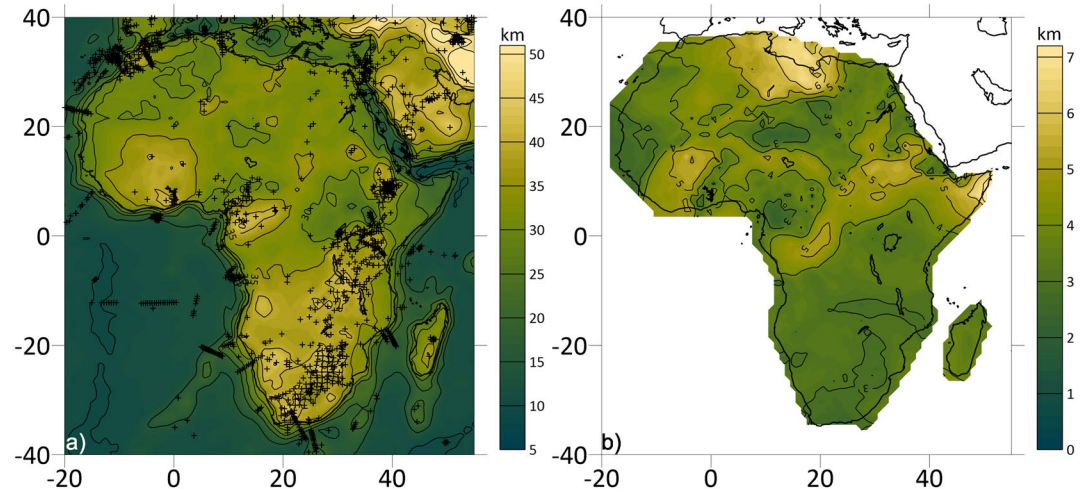
**Figure 3.** (a) Location of seismic measurements and interpolated depth to the Moho. Southern West African craton, northern Congo craton, and most of central to southern Africa show depths to the Moho above 35 km. Opposite to the expectations, a rather thin crust is indicated by depth to Moho around 30 km in northern West African craton and central Congo craton. (b) Interpolation uncertainty of the continental area. As expected, highest values occur in areas of scarce data, like northern West African craton or Horn of Africa, and in the East African rift system (EARS) region, where measurements are heterogeneous.

be of compositional origin, with negative ones indicating iron depletion. The latter are fitted by increasing Mg# changing the percentage of each mineral phase toward those of a strongly iron depleted mantle with Mg# 94, consisting of 69.5% Ol, 4% CPX, 21% OPX, and 5.5% Gt (McDonough & Sun, 1995). The best fitting Mg# and composition are determined by linear interpolation between the densities of the two endmember compositions. In this sense, an increase of Mg# by 1 equals a compositionally induced density decrease of the mineral assembly by ~0.01625 g/cm³. The next iteration starts by recalculating temperatures and thermal density variations based on the adapted composition. Convergence is reached when the maximum difference in Mg# of two subsequent compositional models is ≤0.1 at any grid point. This is usually achieved after four iterations.

The final upper mantle model consists of six grids of 1° lateral resolution at depths of 50, 100, 150, 200, 250, and 300 km for each of temperature, thermal and compositional density variation, and Mg#. Each grid represents the center of a 50 km thick layer, except the topmost one, for which the upper boundary and thus thickness is defined by depth to the Moho. Resulting density variations for the additional layer centered at 15 km are used to improve the crustal density model. For further details of the method, the interested reader is referred to Kaban et al. (2014) and Tesauro et al. (2014a). Details on the regularization term included in the inversion are given in the supplemental material of Kaban et al. (2015).

## 3. Results

### 3.1. Depth to the Moho

Depth to the Moho (Figure 3) varies across the African continent and its patterns partially depend on the distribution of available seismic data. In southern Africa and along the EARS, measurement and/or station density are high and mostly result in depths to the Moho ranging from 35 to 42 km. For most of the Saharan areas, data are very scarce and results are mostly between 28 and 35 km. Similarly differences are also found across cratons. While values in the southern West African craton are greater than 35 km, estimates in its northern part, where no data are available, range from 28 to 32 km. Comparably, depth to the Moho is estimated to lie between 26 and 33 km for the Uganda craton and northeastern to central-western data devoid area of the Congo craton. Meanwhile, interpolation results are above 35 km for the northwestern and southern Congo craton. The well-covered Tanzania, Zimbabwe, and Kaapvaal cratons mostly yield results from 35 to 42 km. A small minimum of 34 km is located in the southern Kaapvaal craton. Overall minimal values on the continent are <25 km in the northern EARS, supported by data, and toward the Horn of Africa, with no data. The latter are most probably an artifact from interpolation between thin oceanic crust in the East and >35 km thick crust at the EARS to the West.
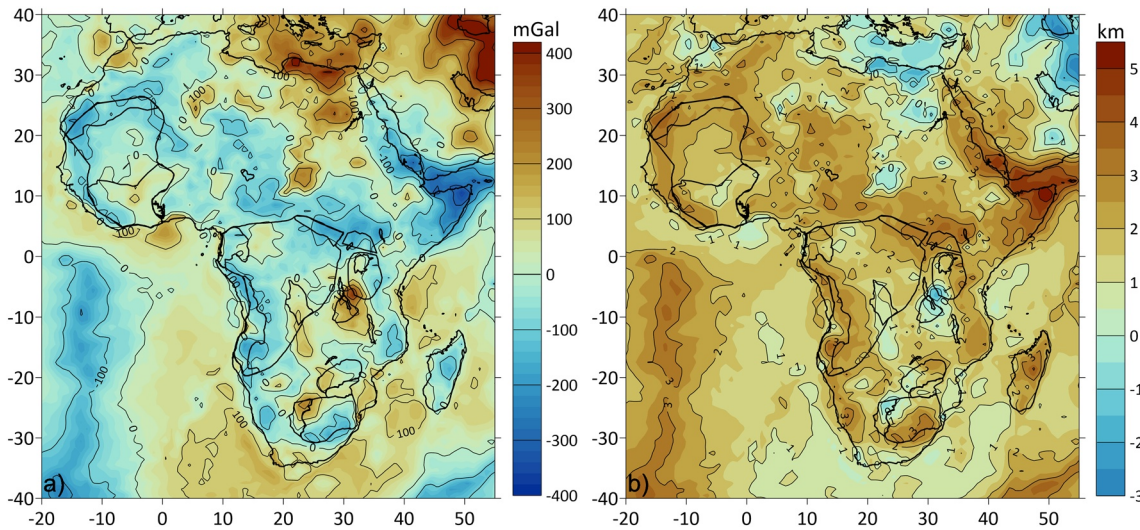
**Figure 4.** Residual mantle gravity (a) and residual topography (b). Extreme values at the Horn of Africa are the result of too thin interpolated depth to Moho due to a lack of data in the region.

As expected based on the high data density, interpolation uncertainties south of the equator are rather small, mostly ranging from 2.8 to 3.6 km, except for the central Congo craton. From here, a band of uncertainties from 4 to some 5 km stretches roughly east and north toward the Horn of Africa, containing the mostly data devoid areas in central Africa. North of the equator, low uncertainties <3 km are present in the well-covered northwestern Congo craton, central Sahara, and west of the West African craton. Uncertainties in the West African craton itself are around 4 km, with maxima of more than 5 km in its South and Northeast. Highest values are >6 km and located at the Horn of Africa and the central part of the Mediterranean coast.

### 3.2. Mantle Residuals

Residual mantle gravity and residual topography (assuming a reference density of 2.67 g/cm³), corrected for deep mantle variations, are shown in Figure 4. As expected, the two fields appear anticorrelated. West African and Congo cratons are dominated by negative gravity residuals partially <−100 mGal with some positive values mostly less than 100 mGal in southern West African craton and northern and eastern Congo craton. Residual topography is lower than 2 km in the central regions and mostly below 3 km toward the respective eastern and western cratonic borders. The same range of values is observed for the Uganda and Tanzania cratons. Meanwhile, southern Zimbabwe craton to northern Kaapvaal craton show positive gravity residuals up to some 200 mGal in northwestern Kaapvaal craton. These are accompanied by residual topography ranging from <2 km to even negative values where highest gravity residuals are observed. In contrast, negative gravity residuals down to −150 mGal and residual topography up to some 3 km are found at southern Kaapvaal craton, while values at northern Zimbabwe craton are in the same range as in the other cratons. At the Horn of Africa, large negative gravity residuals as low as −340 mGal and high residual topography exceeding 5 km confirm that the interpolated values for depth to the Moho in this region are too low.

### 3.3. Mantle

Final results for temperature, thermal and compositional density variations as well as Mg# are presented in Figure 5. Although the modeling approach yields results from the Moho to a depth of 325 km, presentation is limited to the three layers centered at 100, 150, and 200 km depths. Results at shallow depths are strongly affected by possible uncertainties depth to Moho, while no significant compositional variations are expected at larger depths (Begg et al., 2009; Tesauro et al., 2014a). Thus, temperatures and density variations at 50, 250, and 300 km are omitted here. Density variations at 50 km are assessed later for possible adaptation of depth
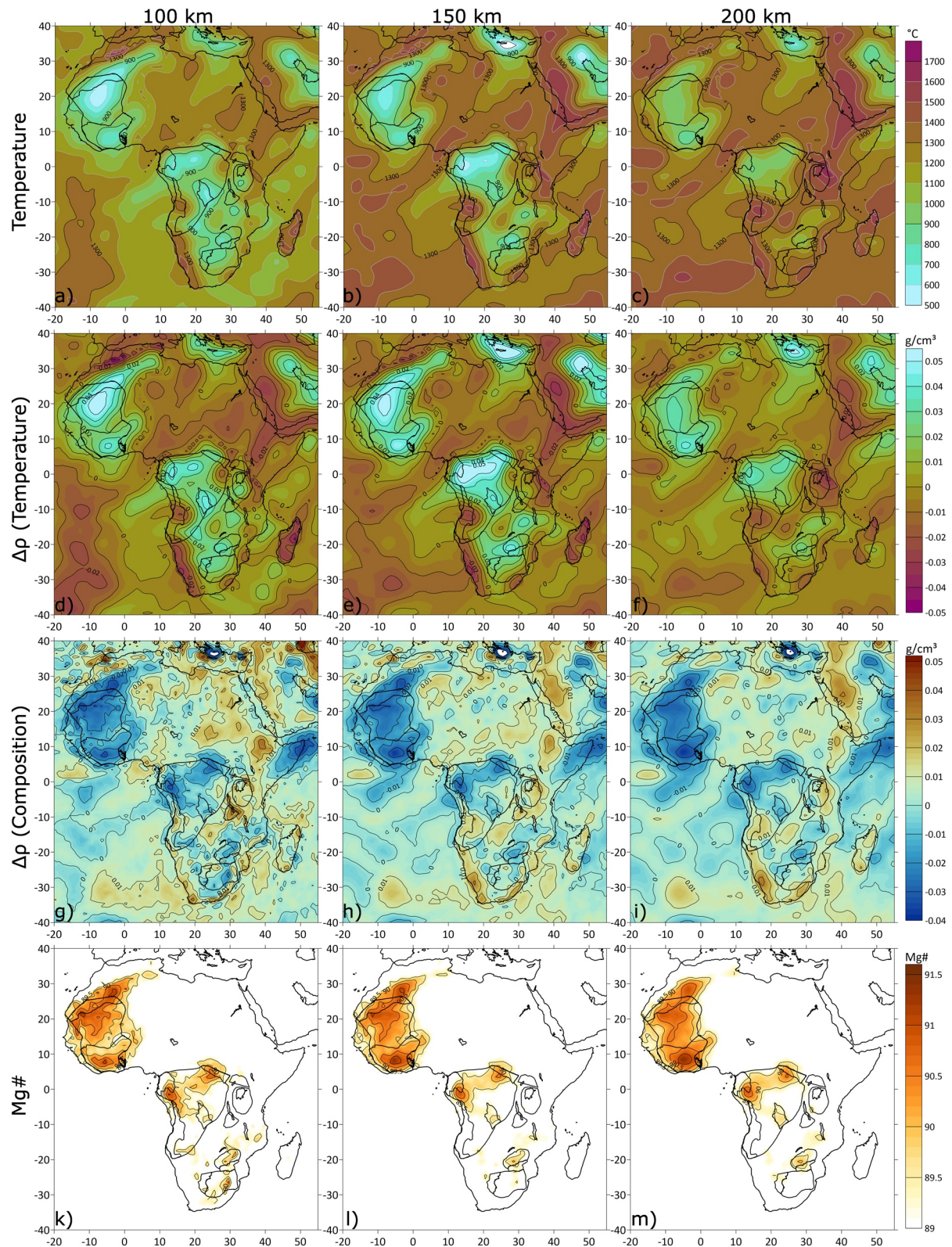
**Figure 5.** Final results from the iterative approach for temperature (a–c), thermal (d–f) and compositional (g–i) density variations, and Mg# (k–m) at depths of 100, 150, and 200 km (columns from left to right). Deep depleted roots are found under the West African, northern and central eastern Congo, and Zimbabwe cratons. They are absent or have been reworked at southern and easternmost Congo, Kaapvaal, Tanzania, and Uganda cratons. There is no evidence that the Bangweulu Block ever developed such a cratonic root. To ease comparison, the same color bars are used for Figures 7 and 9.
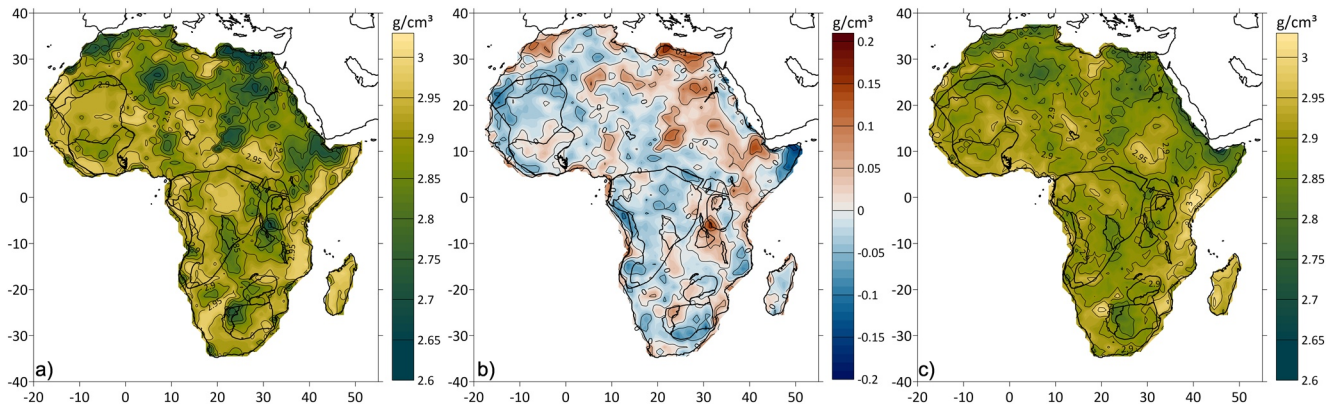
**Figure 6.** Improvement of average crustal density. (a) Initial average crustal density from LITHO1.0 (Pasyanos et al., 2014). (b) Density variations for the crust from the joint inversion. (c) Sum of (a, b), giving an improved average crustal density. (a, c) use the same color scale. In general, adding the density variations leads to a smoother, less heterogeneous crystalline crust density model.

to the Moho. Results at great depths are included in the published data (Finger, Kaban, Tesauro, Mooney, & Thomas, 2021).

At 100 km depth in the area of interest, temperatures below 1000°C are present in most cratonic areas except Uganda craton and parts of Tanzania craton close to the EARS. Lowest values are found in the West African (<600°C) and northern to central Congo cratons (<700°C). Here, temperatures are less than 1100°C to a depth of 200 km. In respect, strong thermal density variations up to more than 0.05 g/cm³ occur in these areas. Low temperatures occur as well at 100 km depth beneath the southern cratons with a minimum of about 800°C in the Zimbabwe craton. They rise with increasing depth, yielding a minimum of about 1100°C at 200 km depth and beyond 1300°C at the southern Kaapvaal craton. Thus, existing positive thermal density variations are less high (up to 0.04 g/cm³), and accompanied by some negative values in the high temperature areas at 200 km depth. The Saharan area not included in the West African craton, the EARS, southern Congo craton, and western coast south of it are marked by high temperatures through depths, partially exceeding 1300°C at 100 km. At 150 km and below, temperatures above 1300°C of the EARS extend under the Uganda and Tanzania cratons. In consequence, thermal density variations are negative in most of those areas at depths below 150 km.

High positive thermal density variations from low temperatures are compensated by negative compositional density variations and thus an increase in Mg#. These patterns are predominant in the West African, central to northern Congo, and Zimbabwe cratons at all depths. In the first, said pattern extends further northeast than one would expect based on the surface geology. In contrast, the eastern and southern Congo, Uganda, and Tanzania cratons are dominated by positive compositional variations, and no increase in Mg#. At Kaapvaal craton, negative compositional variations and increased Mg# exist at 100 km depth but retreat at larger depths, being mostly absent at 200 km.

### 3.4. Improvement of the Average Crustal Density

As mentioned above, the topmost layer of the joint inversion is centered at 15 km depth and thus reveals density variations not included in the initially assumed average density of the crystalline crust taken from LITHO1.0 (Pasyanos et al., 2014). Therefore, their sum yields an improved average crustal density (Figure 6). The initial field (Figure 6a) is very heterogeneous with strong gradients, for example, between the Tanzania craton and Bangweulu block and at northwestern Kaapvaal craton. Furthermore, several regions in the Saharan domain and the two regions just mentioned exhibit unlikely low average crustal densities less than 2.7 g/cm³. In contrast, initial average density of the crust in most cratonic areas is around 2.9 g/cm³, reaching 2.97 g/cm³. Values less than 2.85 g/cm³ are seldom observed. The inverted density variations (Figure 6b) suggest density decreases up to 0.05 g/cm³ for most cratonic areas. Density increases are suggested for cratonic areas with densities around or below 2.85 g/cm³ in the initial model. The modeling results further indicate density increases for low density parts of the Saharan domain and EARS, especially where initial densities are notably low. Therefore, the improved

density model (Figure 6c) is smoother. The cratonic regions are now dominated by densities of 2.85–2.92 g/cm³, with some local minima down to 2.83 g/cm³. Anomalously low crustal densities in other areas of the initial model were increased to densities at least >2.75 g/cm³. Some high densities >2.9 g/cm³ of the initial model are confirmed for the central and northern Sahara, north of the Bomu-Kibali shield, Madagascar, and the eastern coast of Africa.

## 4. Main Sources of Uncertainties and Their Effects on Modeling Results

As mentioned in the previous chapters, the modeling approach requires certain assumptions. For example, the mineralogy is determined by linear interpolation between two end-members representing fertile and depleted mantle conditions, respectively. This way, negative compositional density variations are fitted by an increase in Ol and OPX, a decrease in CPX and Gt. Thus, known aspects of melt depletion processes are considered, for example, that loss of Gt is a main contributor to density loss from melt depletion (Schutt & Lesher, 2006) and that OPX is less stable with fertile compositions at greater depths (Walter, 1998). Yet, the approach cannot take into account all possible phase variations. For example, OPX may also decrease with melt depletion under certain temperature and pressure conditions (Baker, 1994). Moreover, the possible existence of Eclogite, as found in the Superior Craton (Altoe et al., 2020), is not considered in our approach. In any case, the amount of Eclogite in a cratonic mantle should not be significant. Otherwise, Eclogite would compromise a craton's stability due to its high density. In summary, Mg# and the according mineral assembly do not necessarily represent reality, but the quantities best fitting the determined negative density anomalies within the assumed range of mineral phases. Thus, given the variety of factors influencing Mg#, any attempt of quantifying its uncertainties would be unreasonable. However, other main sources of uncertainties and their effects on modeling results are discussed in the following.

### 4.1. Depth to the Moho

The uncertainty of depth to the Moho can have a significant effect on the inversion results. For example, adding the uncertainty to the interpolated Moho depth results in thicker crust which corresponds to less total mass than in the reference model. This causes a smaller crustal gravity correction and higher mantle residuals, respectively. Also, residual topography decreases. At the same time, changing the Moho depth only has a minor effect on the thermal model, since temperatures only change if the assumed composition is changed during iterations. As a reference, Finger, Kaban, Tesauro, Haeger, et al. (2021) only observed differences up to 60 K between their initial and final models. Therefore, an increase in depth to the Moho almost directly translates into higher compositional density variations and lower Mg# in the uppermost mantle, usually balanced by the opposite at greater depths. The described effects are reversed if the crust is thinned, that is, lower compositional variations and thus higher Mg# are expected in the uppermost mantle.

Unfortunately, uncertainties of depth to Moho determinations are not always available. Comparisons in previous works (e.g., Globig et al., 2016; Jessell et al., 2016) show that most Moho depth models differ by less than 10% in areas well-covered by seismic measurements, but differences as high as 25% can occur in data devoid areas. It has to be considered that these are maximum differences between models which stem from the use of different methods and data. Thus, possible uncertainties of the depth to Moho model presented here should be considerably smaller. We use the interpolation uncertainty (Figure 3b) as a basis to assess the effects of depth to Moho uncertainties on the mantle model. In two test cases, the interpolation uncertainty is added to $M_{down}$, right column in Figure 7 and subtracted from $M_{up}$, left column in Figure 7 interpolated depth to the Moho ($M_{base}$). Residual topography and residual mantle gravity are corrected accordingly before the iterative scheme is applied. As expected, the resulting temperature fields at 100 km depth are almost indistinguishable (Figures 7a–7c). Minor differences can be spotted in the southern West African and northern Congo cratons by slight changes in the shape of the 700°C isoline. The subtle changes to the mantle model by shifting the Moho are better visible in the compositional density variations (Figures 7d–7f), for example, by a larger extent of negative values (blue colors) with thinner crust. Yet, absolute differences to the final model are less than 0.01 g/cm³ for both test cases, respectively. Thus, none of the model's results are contradicted, rather confirmed. The extent of depletion with Mg# > 89.5 in the West African craton is larger than the proposed based on surface geology, especially in its
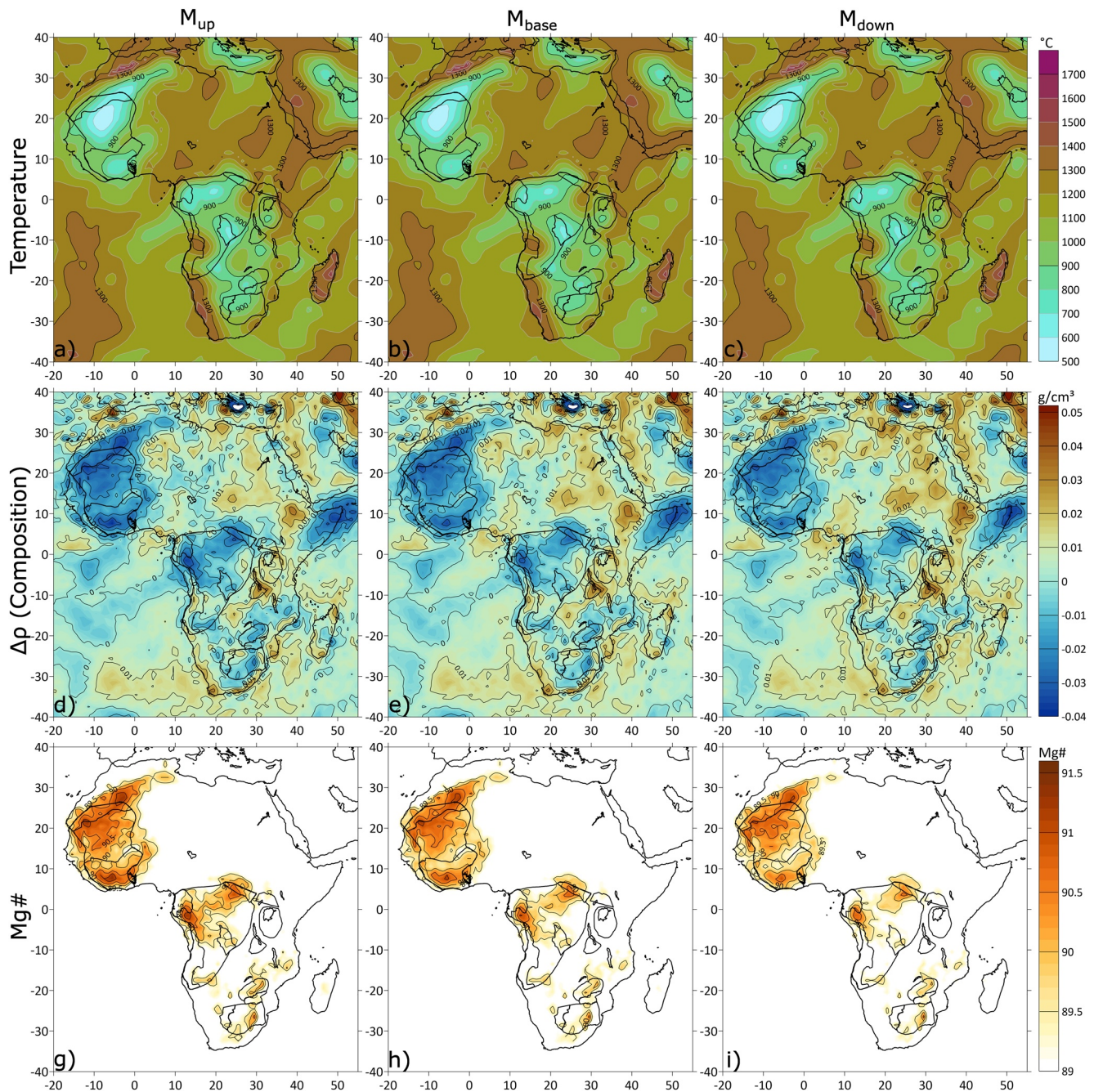
**Figure 7.** Temperatures (a–c), compositional variations (d–f), and Mg# (g–i) at 100 km depth for three scenarios of depth to Moho. Left and right columns show results for depth to Moho shifted upwards ($M_{up}$) and downwards ($M_{down}$), respectively, by subtraction/addition of interpolation uncertainties (Figure 3b). Model results from Figure 5 (left column) are given in the middle column for comparison. Note increased extent and amplitude of negative compositional variations and Mg# for $M_{up}$, and a corresponding decrease for $M_{down}$. Color bars are the same as in Figures 5 and 9.

Northeast. Moreover, the two separate areas with Mg# > 90.5 are present in its North and South in both the cases. Likewise, the Congo craton shows two areas of Mg# > 90 in the Northwest and Northeast, which appear to be not connected by Mg# > 89.5 for $M_{down}$. All other occurrences of increased Mg# are confirmed with slightly larger extents and values for $M_{up}$ and smaller extents and values for $M_{down}$, respectively.

Due to the absence of Moho determinations in wide parts of West African and Congo cratons, it can be assumed that a significant portion of the uppermost mantle density variations (the layer centered at 50 km) is actually
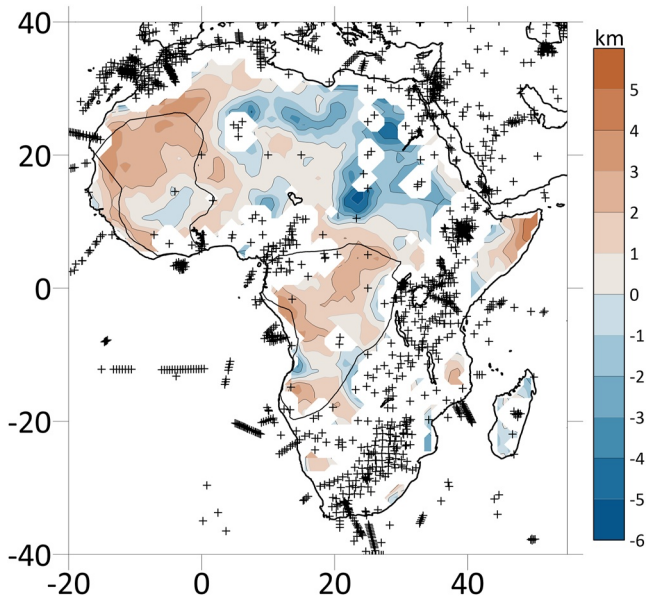
**Figure 8.** Indicated change of depth to the Moho, if all non-thermal density variations in the uppermost mantle were attributed to incorrect placement of the Moho discontinuity. Areas outside continental Africa and in vicinity of sufficient amount of stations (see text) are blanked. As indicated by the red colors, interpolated depth to the Moho is probably too low in wide parts of the Congo and West African cratons. High values at the Horn of Africa confirm that interpolated depth to Moho is too shallow in the area.

caused by unmapped undulations of the Moho discontinuity. Thus, simply multiplying the compositional density variations with the quotient of layer thickness (50 km) and difference of average crustal and subcrustal densities (i.e., $-0.47$ g/cm³) gives an estimate how the Moho depth would need to be modified to accommodate those density variations (Figure 8). It has to be noted, however, that this assumption is only valid in areas not sufficiently covered by seismic measurements. Otherwise, effects of Moho undulations should be minor compared to actual density variations. Therefore, points with less than two measurements within a radius of two degrees are blanked. For wide parts of West African and Congo cratons, increases (red colors) of depth to the Moho up to some 3.5 km are indicated. Values vary between $-1$ and 1 km in the southern West African craton. Some negative values also occur at the southwestern and eastern rims of Congo craton. This strongly indicates that interpolated depth to the Moho is too shallow for most of the two cratons. It has to be considered that the proposed increments of depth to the Moho are related to negative density variations, which are generally expected in cratonic areas. Thus, the proposed increments of up to 3.5 km may provide an overestimate. Since they are mostly smaller than the interpolation uncertainty (Figure 3b), the scenarios $M_{down}$ and $M_{up}$ give a realistic range of possible uncertainties related to the Moho depth interpolation. Due to the increase of depth to the Moho in most of the West African and Congo cratons, $M_{down}$ constitutes a more likely scenario than $M_{up}$ for these cratons.

### 4.2. Tomography and Its Conversion to Temperature

The mineral physics approach used for conversion of S-wave velocities to temperatures are influenced by various uncertainties, as described in previous studies (Finger, Kaban, Tesauro, Haeger, et al., 2021; Haeger et al., 2019; Tesauro et al., 2014a). First, the exact mantle composition is unknown since in-situ measurements are impossible. The use of an incorrect composition can induce errors up to 200°C in highly depleted cratonic areas (Lee, 2003). In this study, uncertainties should be around 100°C, since only medium depletion is observed. Furthermore, the iteratively adjusted compositional model allows to mitigate this effect. In regions of temperatures above 900°C, attenuation can cause errors around 100°C (Jackson et al., 2002). This effect should be reduced by applying the attenuation models *Q3* and *Q4* from Cammarano et al. (2003) as described above. In addition, uncertainties of about 70°C are related to the elastic parameters and their temperature derivatives (Tesauro et al., 2014a). Finally, the underlying S-wave tomography bears its own uncertainties that could cause substantial changes to the resulting temperature model. For example, 50 m/s velocity change, which is, depending on depth, about 1.1% of the reference S-wave velocity, can cause temperature changes of about 100°C (Finger, Kaban, Tesauro, Haeger, et al., 2021). Unfortunately, most tomographic studies do not provide uncertainties for their results. Instead, authors commonly use spike-tests, checkerboard-tests, or synthetic models to test the resolution capacities of their models. Deviation from reference Versus seldom exceeds $-8$ to $+8\%$ in the tomography used here (Celli et al., 2020). Thus, a variation of 50 m/s already constitutes close to 7% of the observed velocity range. Consequently, uncertainties induced by the tomographic model should be smaller than 200°C as long as its own uncertainty remains below 14% of the observed Versus range. In summary, assuming that some of the named error sources are mitigated by the model parametrization as described above, or may counteract each other, resulting temperature uncertainties should generally be less than 200°C.

### 5. Discussion

The models presented here only reflect the current state of the mantle lithosphere. They do not allow to directly determine how or when cratonic roots have been modified, refertilized, destroyed, or if thick lithosphere previously existed. Luckily, diamondiferous kimberlites can work as proxies for the state of the lithosphere at specific times. Conveniently, sub-cratonic mantle provides the necessary temperature and pressure conditions as well as

sufficiently thick lithosphere for the formation of diamondiferous kimberlites. Such kimberlites are discovered and have been analyzed on most African cratons (Begg et al., 2009; De Wit et al., 2016; Faure et al., 2011; Tappe et al., 2018).

In general, our results correspond well to other thermo-compositional models of the lithospheric mantle, for example, WINTERC-G (Fullea et al., 2021) and LithoRef18 (Afonso et al., 2019), despite different modeling assumptions and methodologies. For example, both previous models find the thickest lithosphere of Africa under the West African, northern to central Congo, and Zimbabwe Cratons, which are the areas showing the lowest temperatures, and thus thickest lithosphere, in the region of interest of this study. Areas of depletion in our model generally match those of WINTERC-G, except for the Kaapvaal and southern Congo Cratons, where we find fertile compositions at depths below 100 km. By determining thermal and compositional density variations, it is possible to identify separate root structures of the African cratons in this study.

### 5.1. West African Craton

Our model indicates temperatures below 1300°C to a depth of 200 km beneath the geologically defined West African craton. Moreover, results showing considerable depletion and temperatures less than 1100°C indicate a larger and different subsurface extent of the West African craton than predicted based on surface geology (Figure 9 AA′ and BB′; Begg et al., 2009; Ennih & Liégeois, 2008). They also confirm hypothesized lithospheric thickness considerably higher than 200 km (Steinberger & Becker, 2018). The inference of a larger extent is further confirmed by the wide area of negative compositional density variations and increased Mg#, respectively. These values indicate that depleted cratonic lithosphere is present north of the Reguibat shield (Begg et al., 2009), but does not reach the Anti Atlas, the northern limit of the West African craton proposed by Ennih and Liégeois (2008). To the Northeast, results confirm that depleted cratonic lithosphere extends up to the Mediterranean Sea (Figure 9 BB′; Celli et al., 2020). Thus, the northern limit of cratonic lithosphere parallels the Atlas Mountains, significantly exceeding the areal extent previously proposed from surface observations (Begg et al., 2009; Ennih & Liégeois, 2008). Despite temperatures still below 1300°C at a depth of 200 km, depletion is negligible below 100 km depth in the most northeastern part. Thus, this part of the cratonic root was widely metasomatized. At its eastern boundary, negative compositional anomalies and increased Mg# terminate against the Tuareg and Nigeria Blocks, in agreement with the results of Jessell et al. (2016). In the West and South, low temperatures, negative compositional anomalies, and increased Mg# are observed up to the Atlantic coast, supporting the hypothesis of a previously larger extent of the West African craton in these directions than at present (Jessell et al., 2016).

At the westernmost parts of the shields, our results differ from those of Celli et al. (2020), who argue for an absence of cratonic roots. Yet, this is no direct contradiction since their assessment is solely based on seismic velocities, whose variations are mostly caused by temperatures and the presence of melts or fluids (Goes et al., 2000). In fact, the amplitude of observed values, especially compositional variations and Mg#, decreases toward the coast. Thus, we argue that the cratonic lithosphere was in parts reworked, metasomatized, and probably thinned, but is still about 200 km thick and depleted.

Finally, previous work did not find evidence for a connection of the northern Reguibat and southern Man-Leo shields at depth (Celli et al., 2020; Jessell et al., 2016). Two distinct local temperature minima under them with slightly higher temperatures in between indicate two separate roots for the West African craton (Figure 9 AA′). This pattern occurs as well in the density variations (thermal and compositional) and Mg# down to 150 km depth. At 200 km, a distinction of two bodies may only be made by means of Mg#. Thus, we conclude that the present-day West African craton originates from the amalgamation of two cratonic bodies, whose separate root structures are preserved.

### 5.2. Congo Craton

Temperatures less than 1300°C down to 200 km in the North and toward the central East of the Congo craton confirm the presence of thick lithosphere (Celli et al., 2020). In the East, toward the Tanzania craton, temperatures are up to 400°C higher than at or close to the northwestern Gabon-Cameroon, northeastern Bomu-Kibali
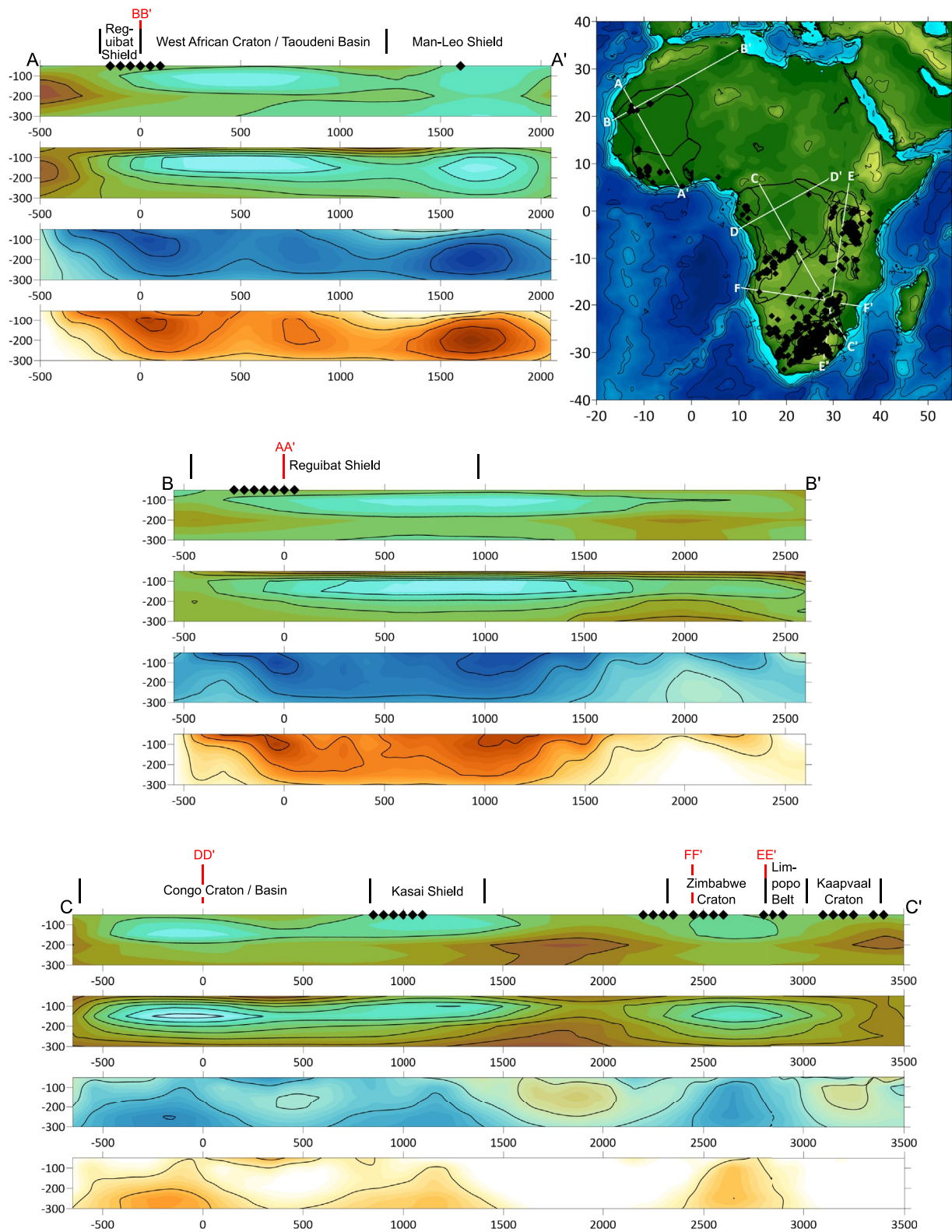
**Figure 9.** 2D profiles through the final mantle models of temperature, thermal density variations, compositional density variations, and Mg# (top to bottom, respectively). For locations of profiles (white lines) and kimberlites (black diamonds, Faure et al., 2011) see inset topography map. Vertical and horizontal axes show depth and location along profile in km, respectively. Black vertical lines above each profile denote the boundaries of cratonic units according to Begg et al. (2009). Red verticals mark intersections with other profiles. Black diamonds denote profile nodes less than 1° away from closest kimberlite location. Profile pairs (AA′ and BB′, CC′, and DD′, as well as EE′ and FF′) intersect orthogonally at profile location km 0. Color bars are the same as in Figures 5 and 7.
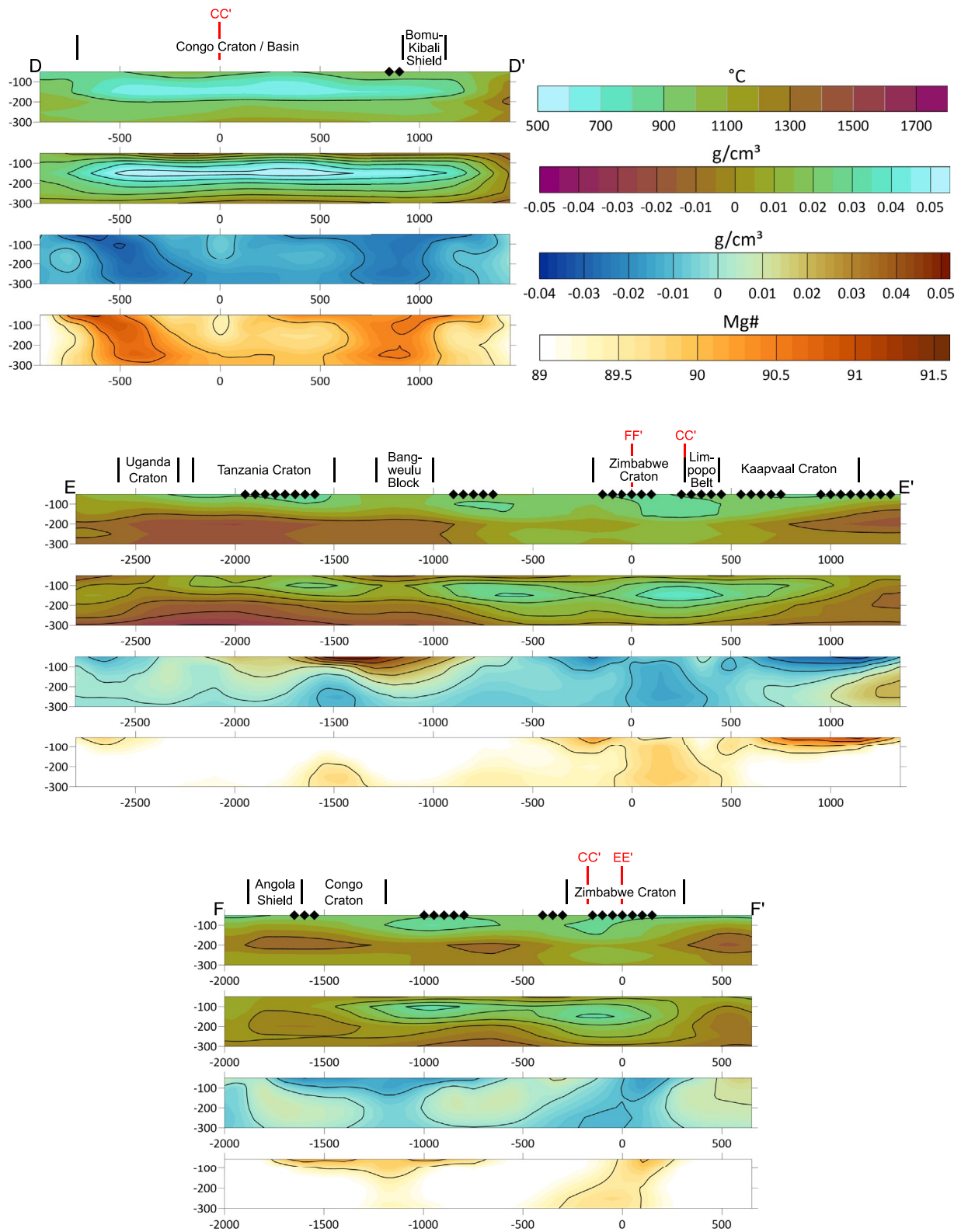
**Figure 9.** (Continued)

and central eastern Kasai shields and exceed 1300°C at 200 km depth. This indicates heating from the East, probably related to the southern end of the EARS. Four local minima of compositional variations and increased Mg# of which those under or at the Gabon-Cameroon, Bomu-Kibali, and Kasai shields persist through depths, confirm the origin of the Congo craton by the amalgamation of separate cratonic terranes (Begg et al., 2009 and references therein). Further, compositional variations and Mg# indicate that the lithosphere of the Gabon-Cameroon and Bomu-Kibali shields was merged into a single block of cold lithosphere during Congo craton formation, but previous root structures were preserved, comparable to the West African craton (Figure 9 AA′ and DD′). Modest negative compositional variations also lead to slightly increased Mg# between the Gabon-Cameroon and Kasai shields (Figure 9 CC′), but are absent between the latter and the Bomu-Kibali shield. Thus, we argue that during the formation of the Congo craton both the Kasai and Bomu-Kibali shields and their roots accreted to the northwestern Gabon-Cameroon shield followed by cooling and thickening of the lithosphere between them. Later, rifting between the Bomu-Kibali and Kasai shields caused the formation of the Congo basin (Delvaux et al., 2021). Subsequent asthenospheric upwelling could have contributed to metasomatization of their lithospheric roots (Maddaloni et al., 2021) and thus extended the area between them where depletion is absent. However, depletion of the roots of the Congo craton shields must have taken place before craton formation. The obtained results also indicate different extents and evolution of the cratonic lithosphere of the Archean shields of the Congo Craton. For the Gabon-Cameroon shield, minimal temperatures are located at its southeastern end, strongly increasing to the Northwest, where they reach up to 1300°C at all depths. In addition, depletion is absent in its northwestern half, although previous presence of thick cratonic lithosphere can be inferred from 2.8 Ga old kimberlites (Tappe et al., 2018). Since its formation, the northern part of the Gabon-Cameroon shield has been subjected to several tectonic processes, possibly including subduction of its northernmost part and subsequent slab detachment (Goussi Ngalamo et al., 2017) that could explain the absence of depletion. Areas of depletion and negative compositional density variations denote a large ovoid NNW–SSE cratonic root under the Gabon-Cameroon shield, stretching along the northern Angola shield, encompassing only its northern tip. Thus, it appears that a depleted cratonic root was already absent under the northern Angola shield at the Congo craton formation. Furthermore, the part of the Congo craton related to the Gabun-Cameroon shield is significantly larger than one would expect from its exposed surface. Variations related to the Bomu-Kibali shield also imply an ovoid depleted root, stretching from beyond its northeastern boundary to the central northern Congo craton. Interestingly, the temperature minimum located closest to the area of strongest depletion of the root is found several hundred km to the West. Minor negative compositional density variations in the East and the abovementioned heating from the EARS indicate reworking of the easternmost Bomu-Kibali lithosphere. To the South, mantle under the Kasai shield appears to be mostly reworked based on up to 200°C higher temperatures, along with less negative compositional density variations and thus lower Mg# that are mostly confined to the shield's surface extent. Below the central Angolan shield, temperatures above 1300°C are found at 100 km depth and dominate the southern Congo craton at a depth of 200 km from the Kasai shield to the Atlantic. Here, depletion is limited to a small area at 100 km depth of southernmost Congo craton (Figure 9 FF′). This is probably a remnant of a depleted cratonic root that was completely removed by the Tristan da Cunha plume (Celli et al., 2020), which is the likely cause of the 135 Ma Paranà-Etendeka flood basalts (Morgan, 1983). Removal of the cratonic root at an earlier time is unlikely, since thick lithosphere was required up to this time based on kimberlite ages of 124–135 Ma (Celli et al., 2020; Tappe et al., 2018). The Etendeka flood basalts located in this area are the counterpart to the South American Parana flood basalts. Thick and depleted lithosphere was found at the Paranapanema craton (Finger, Kaban, Tesauro, Haeger, et al., 2021), where abundant basalts have been erupted. This demonstrates that the eruption and emplacement of large quantities of basaltic magma are not sufficient per se to fully remove a cratonic root. Yet, a strong and long-lasting heat source is able to partially melt such a cratonic root and recycle it into the convecting mantle.

### 5.3. Kaapvaal and Zimbabwe Cratons

Although the isopycnic hypothesis might not be valid for the Kaapvaal craton (Schutt & Lesher, 2010), our obtained results fit well to previous findings. It is evident from several studies (e.g., Brey & Shu, 2018; Griffin, O'Reilly, Natapov, & Ryan, 2003; Lazarov et al., 2009; Sobh et al., 2021; Weiss et al., 2021) that the present-day Kaapvaal craton is the result of several depletion episodes followed by a range of metasomatic refertilizations. Thus, values of Mg# up to 90.5 at 100 km depth probably mark remnants of the depleted cratonic root

(Figure 9 EE′). Since kimberlite compositions confirm the presence of a thick depleted lithosphere up to about 80 Ma (Griffin, O'Reilly, Natapov, & Ryan, 2003), its widespread refertilization must have occurred afterward (Celli et al., 2020). Lithospheric thickness is still debated (e.g., Sodoudi et al., 2013; White-Gaynor et al., 2021), with estimates ranging from up to 300 km (James et al., 2001) to 170 km (Priestley et al., 2008). Concordant with the latter estimate, temperatures close to or above 1300°C deeper than 150 km beneath most parts of the Kaapvaal craton indicate lithosphere thicknesses between 150 and 200 km. At the Zimbabwe craton, depleted cratonic lithosphere appears thick and intact, with temperatures less than 1300°C down to 200 km of depth and Mg# up to 90. However, the imaged area of depletion appears smaller than the cratons surface extent, indicating that the Zimbabwe craton also underwent reworking.

### 5.4. Uganda and Tanzania Craton

Temperatures exceed 1300°C at a depth of 150 km beneath the Uganda and Tanzania cratons. Along with an absence of depletion at all depths this points to complete loss of any previously existing root and a thinned lithosphere (Figure 9 EE′). Yet, temperatures below 1000°C at 100 km depth imply that at least the Tanzania craton was underlain by thick depleted lithosphere until about 30 Ma, close to the time of plume impingement (Rooney, 2017), as confirmed by the age and composition of kimberlites (Gibson et al., 2013; Tappe et al., 2018). The existence of strong cratonic lithosphere at this time would also provide an explanation for the new plate boundary running between the Congo and Tanzania cratons instead of breaking apart the cratonic root of the Tanzania craton. Ongoing lithosphere erosion may be present due to the nearby mantle plume that is responsible for the existence of the EARS. This is indicated by the west-east increasing gradients of temperature and lithospheric thickness estimated in other studies (Boyce et al., 2021; Celli et al., 2020). The Archean Bangweulu microcontinent located southwest of the Tanzania craton appears to exhibit somewhat thicker lithosphere than Uganda and Tanzania cratons as evidenced by temperatures less than 1300°C to a depth of 150 km. Yet, neither estimates of lithospheric depletion nor kimberlites provide evidence that a cratonic root ever existed. If it did, it was eroded completely without presently detectable remnants. Such erosion appears possible in view of the fact that the microcontinent was heavily deformed by the surrounding Proterozoic belts (Begg et al., 2009).

## 6. Conclusions

In this work, recent S-wave tomography was combined with satellite gravity and crustal data to obtain self-consistent models of temperatures, thermal and compositional density variations, and Mg# for the African upper mantle down to 325 km, focusing on its cratonic parts. In addition, a new, purely seismic model of depth to the Moho was calculated and an improved model of average crustal densities obtained. Depth to the Moho is in the range of 35–42 km in most cratonic regions, except the central to northeastern Congo and northern West African cratons. For these regions, mantle modeling results indicated that depths to the Moho, in parts as low as 28 km, are underestimated due to a lack of sufficient seismic measurements. Average crystalline crust densities of the cratonic areas are 2.85–2.92 g/cm³ in most cratonic areas. Lower values (around 2.83 g/cm³) occur at the Reguibat (northern West African craton) and Kasai (eastern Congo craton) shields as well as western Kaapvaal craton. An assessment of the effects of uncertainties in the depth to Moho and the velocity-temperature conversion showed that they do not qualitatively affect the primary results presented here concerning the physical state of the African cratonic roots.

Deep depleted lithospheric roots were found under the Reguibat and Man-Leo shields of the West African craton, the Gabon-Cameroon, Bomu-Kibali, and Kasai shields of the Congo craton and Zimbabwe craton. In these regions, temperatures range from less than 700°C at 100 km depth to less than 1200°C at 200 km depth, accompanied by compositional variations between −0.01 and −0.035 g/cm³, which indicate values of Mg# from 89.5 to 91.4, respectively. The identification of separate cratonic roots under the Archean shields of the Congo and West African cratons provides strong evidence that depletion of these roots occurred before they were amalgamated into the larger cratons. Some depletion was imaged at the southernmost Angolan shield of the Congo craton and at Kaapvaal craton, but vanishes with temperatures exceeding 1300°C at or below 150 km of depth, and is absent beneath the Uganda and Tanzania cratons. Previously existing cratonic roots in these areas were largely reworked or completely removed, the most likely cause being mantle plumes, as evidenced by active volcanism or flood basalts.

## Data Availability Statement

Data associated with this article is available via GFZ Data Services (Finger, Kaban, Tesauro, Mooney, & Thomas, 2021): https://doi.org/10.5880/GFZ.1.3.2021.006.

## References

Afonso, J. C., Salajegheh, F., Szwillus, W., Ebbing, J., & Gaina, C. (2019). A global reference model of the lithosphere and upper mantle from joint inversion and analysis of multiple data sets. *Geophysical Journal International*, *217*(3), 1602–1628. https://doi.org/10.1093/gji/ggz094

Altoe, I., Eeken, T., Goes, S., Foster, A., & Darbyshire, F. (2020). Thermo-compositional structure of the north-eastern Canadian Shield from Rayleigh wave dispersion analysis as a record of its tectonic history. *Earth and Planetary Science Letters*, *547*, 116465. https://doi.org/10.1016/j.epsl.2020.116465

Amante, C., & Eakins, B. W. (2009). ETOPO1 1 Arc-minute global relief model: Procedures, data sources and analysis. NOAA Technical Memorandum NESDIS NGDC-24, (March), p. 19. https://doi.org/10.1594/PANGAEA.769615

Baker, M. B. (1994). The composition of high-pressure mantle melts: Results from diamond aggregate experiments. *Mineralogical Magazine*, *58A*(1), 44–45. https://doi.org/10.1180/minmag.1994.58a.1.26

Begg, G. C., Griffin, W. L., Natapov, L. M., O'Reilly, S. Y., Grand, S. P., O'Neill, C. J., et al. (2009). The lithospheric architecture of Africa: Seismic tomography, mantle petrology, and tectonic evolution. *Geosphere*, *5*(1), 23–50. https://doi.org/10.1130/GES00179.1

Boyce, A., Bastow, I. D., Cottaar, S., Kounoudis, R., Courbeville, J. G. D., Caunt, E., & Desai, S. (2021). AFRP20: New P-wavespeed model for the African mantle reveals two whole-mantle plumes below East Africa and neoproterozoic modification of the Tanzania craton. *Geochemistry, Geophysics, Geosystems*, *22*(3), e2020GC009302. https://doi.org/10.1029/2020GC009302

Brey, G. P., & Shu, Q. (2018). The birth, growth and ageing of the Kaapvaal subcratonic mantle. *Mineralogy and Petrology*, *112*(1), 23–41. https://doi.org/10.1007/S00710-018-0577-8

Cammarano, F., Goes, S., Vacher, P., & Giardini, D. (2003). Inferring upper-mantle temperatures from seismic velocities. *Physics of the Earth and Planetary Interiors*, *138*(3–4), 197–222. https://doi.org/10.1016/S0031-9201(03)00156-0

Celli, N. L., Lebedev, S., Schaeffer, A. J., & Gaina, C. (2020). African cratonic lithosphere carved by mantle plumes. *Nature Communications*, *11*(1), 92. https://doi.org/10.1038/s41467-019-13871-2

Crameri, F., Shephard, G. E., & Heron, P. J. (2020). The misuse of colour in science communication. *Nature Communications*, *11*(1), 1–10. https://doi.org/10.1038/s41467-020-19160-7

Delvaux, D., Maddaloni, F., Tesauro, M., & Braitenberg, C. (2021). The Congo Basin: Stratigraphy and subsurface structure defined by regional seismic reflection, refraction and well data. *Global and Planetary Change*, *198*(December 2020), 103407. https://doi.org/10.1016/j.gloplacha.2020.103407

De Wit, M., Bhebhe, Z., Davidson, J., Haggerty, S. E., Hundt, P., Jacob, J., et al. (2016). Overview of diamond resources in Africa. *Episodes*, *39*(2), 199–237. https://doi.org/10.18814/epiiugs/2016/v39i2/95776

Dziewonski, A. M., & Anderson, D. L. (1981). Preliminary reference Earth model. *Physics of the Earth and Planetary Interiors*, *25*(4), 297–356. https://doi.org/10.1016/0031-9201(81)90046-7

Ebinger, C. J., & Sleep, N. H. (1998). Cenozoic magmatism throughout east Africa resulting from impact of a single plume. *Nature*, *395*(6704), 788–791. https://doi.org/10.1038/27417

Ennih, N., & Liégeois, J.-P. (2008). The boundaries of the West African craton, with special reference to the basement of the Moroccan metacratonic Anti-Atlas belt. *Geological Society, London, Special Publications*, *297*(1), 1–17. https://doi.org/10.1144/SP297.1

Faure, S., Godey, S., Fallara, F., & Trépanier, S. (2011). Seismic architecture of the Archean North American mantle and its relationship to diamondiferous Kimberlite fields. *Economic Geology*, *106*(2), 223–240. https://doi.org/10.2113/ECONGEO.106.2.223

Finger, N.-P., Kaban, M. K., Tesauro, M., Haeger, C., Mooney, W. D., & Thomas, M. (2020). A thermo-compositional model of the cratonic lithosphere of South America: Models of the upper mantle, crust and sediment density. GFZ Data Services. https://doi.org/10.5880/GFZ.1.3.2020.006

Finger, N.-P., Kaban, M. K., Tesauro, M., Haeger, C., Mooney, W. D., & Thomas, M. (2021). A thermo-compositional model of the cratonic lithosphere of South America. *Geochemistry, Geophysics, Geosystems*, *22*(4), e2020GC009307. https://doi.org/10.1029/2020GC009307

Finger, N.-P., Kaban, M. K., Tesauro, M., Mooney, W. D., & Thomas, M. (2021). Thermo-compositional model of cratonic lithosphere and depth to Moho of Africa. GFZ Data Services. https://doi.org/10.5880/GFZ.1.3.2021.006

Fishwick, S. (2010). Surface wave tomography: Imaging of the lithosphere–asthenosphere boundary beneath central and southern Africa? *Lithos*, *120*(1–2), 63–73. https://doi.org/10.1016/J.LITHOS.2010.05.011

Förste, C., Bruinsma, S., Abrikosov, O., Flechtner, F., Marty, J.-C., Lemoine, J.-M., et al. (2014). EIGEN-6C4-The latest combined global gravity field model including GOCE data up to degree and order 1949 of GFZ Potsdam and GRGS Toulouse. Geophysical Research Abstracts (Vol. 16). Retrieved from http://icgem.gfz-potsdam.de

Fullea, J., Lebedev, S., Martinec, Z., & Celli, N. L. (2021). WINTERC-G: Mapping the upper mantle thermochemical heterogeneity from coupled geophysical–petrological inversion of seismic waveforms, heat flow, surface elevation and gravity satellite data. *Geophysical Journal International*, *226*(1), 146–191. https://doi.org/10.1093/gji/ggab094

Gibson, S. A., McMahon, S. C., Day, J. A., & Dawson, J. B. (2013). Highly refractory lithospheric mantle beneath the Tanzanian Craton: Evidence from Lashaine pre-metasomatic garnet-bearing peridotites. *Journal of Petrology*, *54*(8), 1503–1546. https://doi.org/10.1093/PETROLOGY/EGT020

Giuliani, A., Phillips, D., Maas, R., Woodhead, J. D., Kendrick, M. A., Greig, A., et al. (2014). LIMA U–Pb ages link lithospheric mantle metasomatism to Karoo magmatism beneath the Kimberley region, South Africa. *Earth and Planetary Science Letters*, *401*, 132–147. https://doi.org/10.1016/J.EPSL.2014.05.044

Globig, J., Fernàndez, M., Torne, M., Vergés, J., Robert, A., & Faccenna, C. (2016). New insights into the crust and lithospheric mantle structure of Africa from elevation, geoid, and thermal analysis. *Journal of Geophysical Research: Solid Earth*, *121*(7), 5389–5424. https://doi.org/10.1002/2016JB012972

Goes, S., Govers, R., & Vacher, P. (2000). Shallow mantle temperatures under Europe from P and S wave tomography. *Journal of Geophysical Research*, *105*(B5), 11153–11169. https://doi.org/10.1029/1999JB900300

Goussi Ngalamo, J. F., Bisso, D., Abdelsalam, M. G., Atekwana, E. A., Katumwehe, A. B., & Ekodeck, G. E. (2017). Geophysical imaging of metacratonizaton in the northern edge of the Congo craton in Cameroon. *Journal of African Earth Sciences*, *129*, 94–107. https://doi.org/10.1016/J.JAFREARSCI.2016.12.010

Griffin, W. L., O'Reilly, S. Y., Abe, N., Aulbach, S., Davies, R. M., Pearson, N. J., et al. (2003). The origin and evolution of Archean lithospheric mantle. *Precambrian Research*, *127*(1–3), 19–41. https://doi.org/10.1016/S0301-9268(03)00180-3

Griffin, W. L., O'Reilly, S. Y., Natapov, L. M., & Ryan, C. G. (2003). The evolution of lithospheric mantle beneath the Kalahari Craton and its margins. *Lithos*, *71*(2–4), 215–241. https://doi.org/10.1016/J.LITHOS.2003.07.006

Haas, P., Ebbing, J., Celli, N. L., & Rey, P. F. (2021). Two-step gravity inversion reveals variable architecture of African Cratons. *Frontiers in Earth Science*, *9*(December), 1–14. https://doi.org/10.3389/feart.2021.696674

Haeger, C., & Kaban, M. K. (2019). Decompensative gravity anomalies reveal the structure of the upper crust of Antarctica. *Pure and Applied Geophysics*, *176*(10), 4401–4414. https://doi.org/10.1007/s00024-019-02212-5

Haeger, C., Kaban, M. K., Tesauro, M., Petrunin, A. G., & Mooney, W. D. (2019). 3-D density, thermal, and compositional model of the Antarctic lithosphere and implications for its evolution. *Geochemistry, Geophysics, Geosystems*, *20*(2), 688–707. https://doi.org/10.1029/2018GC008033

Hu, J., Liu, L., Faccenda, M., Zhou, Q., Fischer, K. M., Marshak, S., & Lundstrom, C. (2018). Modification of the Western Gondwana craton by plume-lithosphere interaction. *Nature Geoscience*, *11*(3), 203–210. https://doi.org/10.1038/s41561-018-0064-1

Jackson, I., Fitz Gerald, J. D., Faul, U. H., & Tan, B. H. (2002). Grain-size-sensitive seismic wave attenuation in polycrystalline olivine. *Journal of Geophysical Research*, *107*(B12), ECV5-1–ECV5-16. https://doi.org/10.1029/2001jb001225

James, D. E., Fouch, M. J., VanDecar, J. C., & van der Lee, S. (2001). Tectospheric structure beneath southern Africa. *Geophysical Research Letters*, *28*(13), 2485–2488. https://doi.org/10.1029/2000GL012578

Jessell, M. W., Begg, G. C., & Miller, M. S. (2016). The geophysical signatures of the West African Craton. *Precambrian Research*, *274*, 3–24. https://doi.org/10.1016/J.PRECAMRES.2015.08.010

Jordan, T. H. (1978). Composition and development of the continental tectosphere. *Nature*, *274*(5671), 544–548. https://doi.org/10.1038/274544a0

Kaban, M. K., El Khrepy, S., & Al-Arifi, N. (2016). Isostatic model and isostatic gravity anomalies of the Arabian plate and surroundings. *Pure and Applied Geophysics*, *173*(4), 1211–1221. https://doi.org/10.1007/s00024-015-1164-0

Kaban, M. K., El Khrepy, S., Al-Arifi, N., Tesauro, M., & Stolk, W. (2016). Three-dimensional density model of the upper mantle in the Middle East: Interaction of diverse tectonic processes. *Journal of Geophysical Research: Solid Earth*, *121*(7), 5349–5364. https://doi.org/10.1002/2015JB012755

Kaban, M. K., & Mooney, W. D. (2001). Density structure of the lithosphere in the southwestern United States and its tectonic significance. *Journal of Geophysical Research*, *106*(B1), 721–739. https://doi.org/10.1029/2000JB900235

Kaban, M. K., Mooney, W. D., & Petrunin, A. G. (2015). Cratonic root beneath North America shifted by basal drag from the convecting mantle. *Nature Geoscience*, *8*(10), 797–800. https://doi.org/10.1038/ngeo2525

Kaban, M. K., Stolk, W., Tesauro, M., El Khrepy, S., Al-Arifi, N., Beekman, F., & Cloetingh, S. A. P. L. (2016). 3D density model of the upper mantle of Asia based on inversion of gravity and seismic tomography data. *Geochemistry, Geophysics, Geosystems*, *17*(11), 4457–4477. https://doi.org/10.1002/2016GC006458

Kaban, M. K., Tesauro, M., Mooney, W. D., & Cloetingh, S. A. P. L. (2014). Density, temperature, and composition of the North American lithosphere-new insights from a joint analysis of seismic, gravity, and mineral physics data: 1. Density structure of the crust and upper mantle. *Geochemistry, Geophysics, Geosystems*, *15*(12), 4781–4807. https://doi.org/10.1002/2014GC005483

Laske, G., Masters, G., Ma, Z., & Pasyanos, M. (2013). Update on CRUST1.0---A 1-degree global model of Earth's crust. *EGU General Assembly*, *15*, 2658. Retrieved from https://ui.adsabs.harvard.edu/abs/2013EGUGA..15.2658L/abstract

Lazarov, M., Brey, G. P., & Weyer, S. (2009). Time steps of depletion and enrichment in the Kaapvaal craton as recorded by subcalcic garnets from Finsch (SA). *Earth and Planetary Science Letters*, *279*(1–2), 1–10. https://doi.org/10.1016/J.EPSL.2008.12.015

Lee, C.-T. A. (2003). Compositional variation of density and seismic velocities in natural peridotites at STP conditions: Implications for seismic imaging of compositional heterogeneities in the upper mantle. *Journal of Geophysical Research*, *108*(B9). https://doi.org/10.1029/2003jb002413

Lee, C.-T. A., Luffi, P., & Chin, E. J. (2011). Building and destroying continental mantle. *Annual Review of Earth and Planetary Sciences*, *39*(1), 59–90. https://doi.org/10.1146/annurev-earth-040610-133505

Maddaloni, F., Braitenberg, C., Kaban, M. K., Tesauro, M., & Delvaux, D. (2021). The Congo Basin: Subsurface structure interpreted using potential field data and constrained by seismic data. *Global and Planetary Change*, *205*(July), 103611. https://doi.org/10.1016/j.gloplacha.2021.103611

McDonough, W. F., & Sun, S. s. (1995). The composition of the Earth. *Chemical Geology*, *120*(3–4), 223–253. https://doi.org/10.1016/0009-2541(94)00140-4

Mooney, W. D. (2015). Crust and lithospheric structure—Global crustal structure. In G. Schubert, B. Romanowicz, & A. Dziewonski (Eds.), *Treatise on geophysics* (2nd ed., pp. 339–390). Elsevier. https://doi.org/10.1016/b978-0-444-53802-4.00010-5

Mooney, W. D., & Kaban, M. K. (2010). The North American upper mantle: Density, composition, and evolution. *Journal of Geophysical Research*, *115*(B12), B12424. https://doi.org/10.1029/2010JB000866

Mooney, W. D., & Vidale, J. E. (2003). Thermal and chemical variations in subcrustal cratonic lithosphere: Evidence from crustal isostasy. *Lithos*, *71*(2–4), 185–193. https://doi.org/10.1016/J.LITHOS.2003.07.004

Morgan, W. J. (1983). Hotspot tracks and the early rifting of the Atlantic. *Developments in Geotectonics*, *19*(C), 123–139. https://doi.org/10.1016/B978-0-444-42198-2.50015-8

Murphy, B., Müller, S., & Yurchak, R. (2020). GeoStat-framework/PyKrige: v1.5.0. https://doi.org/10.5281/ZENODO.3739879

Pasyanos, M. E., Masters, T. G., Laske, G., & Ma, Z. (2014). LITHO1.0: An updated crust and lithospheric model of the Earth. *Journal of Geophysical Research: Solid Earth*, *119*(3), 2153–2173. https://doi.org/10.1002/2013JB010626

Pasyanos, M. E., & Nyblade, A. A. (2006). A top to bottom lithospheric study of Africa and Arabia. *Tectonophysics*, *444*(1–4), 27–44. https://doi.org/10.1016/J.TECTO.2007.07.008

Priestley, K., Mckenzie, D., Debayle, E., & Pilidou, S. (2008). The African upper mantle and its relationship to tectonics and surface geology. *Geophysical Journal International*, *175*(3), 1108–1126. https://doi.org/10.1111/J.1365-246X.2008.03951.X

Ritsema, J., Deuss, A., van Heijst, H. J., & Woodhouse, J. H. (2011). S40RTS: A degree-40 shear-velocity model for the mantle from new Rayleigh wave dispersion, teleseismic traveltime and normal-mode splitting function measurements. *Geophysical Journal International*, *184*(3), 1223–1236. https://doi.org/10.1111/j.1365-246X.2010.04884.x

Rooney, T. O. (2017). The Cenozoic magmatism of East-Africa: Part I—Flood basalts and pulsed magmatism. *Lithos*, *286–287*, 264–301. https://doi.org/10.1016/J.LITHOS.2017.05.014

Root, B. C., Novák, P., Dirkx, D., Kaban, M. K., van der Wal, W., & Vermeersen, L. L. A. (2016). On a spectral method for forward gravity field modelling. *Journal of Geodynamics*, *97*, 22–30. https://doi.org/10.1016/J.JOG.2016.02.008

Schaeffer, A. J., & Lebedev, S. (2013). Global shear speed structure of the upper mantle and transition zone. *Geophysical Journal International*, *194*(1), 417–449. https://doi.org/10.1093/gji/ggt095

Schutt, D. L., & Lesher, C. E. (2006). Effects of melt depletion on the density and seismic velocity of garnet and spinel lherzolite. *Journal of Geophysical Research*, *111*(5), 1–24. https://doi.org/10.1029/2003JB002950

Schutt, D. L., & Lesher, C. E. (2010). Compositional trends among Kaapvaal Craton garnet peridotite xenoliths and their effects on seismic velocity and density. *Earth and Planetary Science Letters*, *300*(3–4), 367–373. https://doi.org/10.1016/j.epsl.2010.10.018

Sobh, M., Gerhards, C., Fadel, I., & Götze, H. J. (2021). Mapping the thermal structure of Southern Africa from Curie depth estimates based on wavelet analysis of magnetic data with uncertainties. *Geochemistry, Geophysics, Geosystems*, *22*(11), 1–22. https://doi.org/10.1029/2021GC010041

Sodoudi, F., Yuan, X., Kind, R., Lebedev, S., Adam, J. M. C., Kästle, E., & Tilmann, F. (2013). Seismic evidence for stratification in composition and anisotropic fabric within the thick lithosphere of Kalahari Craton. *Geochemistry, Geophysics, Geosystems*, *14*(12), 5393–5412. https://doi.org/10.1002/2013GC004955

Steinberger, B., & Becker, T. W. (2018). A comparison of lithospheric thickness models. *Tectonophysics*, *746*, 325–338. https://doi.org/10.1016/j.tecto.2016.08.001

Stixrude, L., & Lithgow-Bertelloni, C. (2005). Thermodynamics of mantle minerals—I. Physical properties. *Geophysical Journal International*. Narnia, *162*, 610–632. https://doi.org/10.1111/j.1365-246X.2005.02642.x

Stolk, W., Kaban, M. K., Beekman, F., Tesauro, M., Mooney, W. D., & Cloetingh, S. (2013). High resolution regional crustal models from irregularly distributed data: Application to Asia and adjacent areas. *Tectonophysics*, *602*, 55–68. https://doi.org/10.1016/j.tecto.2013.01.022

Tappe, S., Smart, K., Torsvik, T., Massuyeau, M., & de Wit, M. (2018). Geodynamics of kimberlites on a cooling Earth: Clues to plate tectonic evolution and deep volatile cycles. *Earth and Planetary Science Letters*, *484*, 1–14. https://doi.org/10.1016/j.epsl.2017.12.013

Tesauro, M., Kaban, M. K., & Aitken, A. R. A. (2020). Thermal and compositional anomalies of the Australian upper mantle from seismic and gravity data. *Geochemistry, Geophysics, Geosystems*, *21*(11), e2020GC009305. https://doi.org/10.1029/2020GC009305

Tesauro, M., Kaban, M. K., Mooney, W. D., & Cloetingh, S. A. P. L. (2014b). NACr14: A 3D model for the crustal structure of the North American continent. *Tectonophysics*, *631*, 65–86. https://doi.org/10.1016/j.tecto.2014.04.016

Tesauro, M., Kaban, M. K., Mooney, W. D., & Cloetingh, S. A. P. L. (2014a). Density, temperature, and composition of the North American lithosphere-New insights from a joint analysis of seismic, gravity, and mineral physics data: 2. Thermal and compositional model of the upper mantle. *Geochemistry, Geophysics, Geosystems*, *15*(12), 4808–4830. https://doi.org/10.1002/2014GC005484

Tugume, F., Nyblade, A., Julià, J., & van der Meijde, M. (2013). Precambrian crustal structure in Africa and Arabia: Evidence lacking for secular variation. *Tectonophysics*, *609*, 250–266. https://doi.org/10.1016/J.TECTO.2013.04.027

van der Meijde, M., Fadel, I., Ditmar, P., & Hamayun, M. (2015). Uncertainties in crustal thickness models for data sparse environments: A review for South America and Africa. *Journal of Geodynamics*, *84*, 1–18. https://doi.org/10.1016/J.JOG.2014.09.013

Walter, M. (1998). Melting of garnet peridotite and the origin of Komatiite and depleted lithosphere. *Journal of Petrology*, *39*(1), 29–60. https://doi.org/10.1093/petroj/39.1.29

Weiss, Y., Kiro, Y., Class, C., Winckler, G., Harris, J. W., & Goldstein, S. L. (2021). Helium in diamonds unravels over a billion years of craton metasomatism. *Nature Communications*, *12*(11), 1–11. https://doi.org/10.1038/s41467-021-22860-3

White-Gaynor, A. L., Nyblade, A. A., Durrheim, R. J., Raveloson, R., van der Meijde, M., Fadel, I., et al. (2021). Shear-wave velocity structure of the Southern African upper mantle: Implications for craton structure and plateau uplift. *Geophysical Research Letters*, *48*(7), e2020GL091624. https://doi.org/10.1029/2020GL091624

Wilson, M. (1997). Thermal evolution of the Central Atlantic passive margins: Continental break-up above a Mesozoic super-plume. *Journal of the Geological Society*, *154*(3), 491–495. https://doi.org/10.1144/gsjgs.154.3.0491